Available online at www.sciencedirect.com
SCIENCE DIRECT
Journal of Catalysis 229 (2005) 163–175
JOURNAL OF CATALYSIS
www.elsevier.com/locate/jcat

# Mechanistic features for propane reforming by carbon dioxide over a Ni/Mg(Al)O hydrotalcite-derived catalyst

A. Olafsen [a], Å. Slagtern [a], I.M. Dahl [a], U. Olsbye [b,*], Y. Schuurman [c], C. Mirodatos [c]

[a] *SINTEF Materials and Chemistry, P.O. Box 124 Blindern, N-0314 Oslo, Norway*
[b] *Department of Chemistry, Center for Materials Science and Nanotechnology, University of Oslo, P.O. Box 1033 Blindern, N-0315 Oslo, Norway*
[c] *Institut de Recherches sur la Catalyse, CNRS, 2 Avenue Albert Einstein, F-69626 Villeurbanne cedex, France*

Received 16 May 2004; revised 30 September 2004; accepted 1 October 2004

Available online 8 December 2004

**Abstract**

A 1.9 wt% Ni/Mg(Al)O hydrotalcite-derived catalyst is studied for the dry reforming of propane to synthesis gas at 600 °C and 1 atm. The catalyst showed limited initial deactivation and then was exceptionally stable throughout a 34-day test. Catalyst characterisation indicates that the carrier material consists of a mixed Mg(Al)O phase before and after testing, and that carbonate forms on the support surface under dry reforming conditions. The Ni particles are in close contact with, and partially decorated by, the basic support. No carbon whisker formation is observed by transmission electron microscopy after catalytic testing.

Alternating pulse experiments in a Temporary Analysis of Product-II (TAP-II) reactor system indicate that $CO_2$ is associatively adsorbed on the basic Mg(Al)O carrier and acts as a permanent source of oxygen species for the Ni metal. Propane reacts rapidly with Ni–O species to form CO and $H_2O$. Under TAP conditions, reduced Ni reacts gradually with carbonate from the support to give Ni–O species and CO.


*Keywords:* $CO_2$ reforming; Propane; Hydrotalcite; Mechanistic study; Magnetic measurements; DRIFTS; TAP; TEM; Metal–support interaction

## 1. Introduction

Natural gas (NG) from the North Sea contains ca. 10 vol% light alkanes ($C_2$–$C_4$). Conversion of NG into more valuable products by reforming reactions is of major importance. Light alkanes also have a high potential for use as fuel in modern compact fuel reformers. Overall detailed understanding of the catalytic (pre-)reforming processes is required to develop high-performance catalysts for such reactions, that is, catalysts with a high activity and selectivity for the target products, CO and $H_2$, and with a low selectivity for coke formation.

During the past three decades, several groups have reported catalytic results for the wet or dry reforming of methane to synthesis gas over Ni/Mg(Al)O catalysts based on hydrotalcite-like precursors. It is generally agreed that Ni/Mg(Al)O is a very active catalyst for methane reforming, most likely because of an optimum combination of basicity of the support, metal particle size, and/or an electronic "spillover" effect of the carrier material (see, e.g., [1–3] and references therein). To our knowledge, no one has yet exploited a fourth possibility in any detail, that is, a possible direct participation of the hydrotalcite-like carrier material in the reaction cycle.

There are numerous articles on the catalytic dry reforming of methane to synthesis gas, and some selected works are described in Section 4. A literature search for propane dry reforming revealed only two mechanistic studies, both using supported noble metal catalysts (Rh, Ru) [4,5]. In [4], Solymosi et al. used FT-IR spectroscopy and reactor studies to investigate the dry reforming of propane over Rh on various supports. They reported the formation of propene and propylidyne species on the catalysts during the propane dissociation reaction even at low temperatures (250–300 K).

* Corresponding author. Fax: + 4722855441.
*E-mail address:* unni.olsbye@kjemi.uio.no (U. Olsbye).

0021-9517/$ – see front matter 
doi:10.1016/j.jcat.2004.10.002

Addition of $CO_2$ to the feed led to rapid reaction with either propane or propene on the catalyst, yielding synthesis gas as the major product. Partial pressure variations at 550–650 °C indicated that $CO_2$ is involved in the rate-determining step of the reaction. Sutton et al. [5] performed a kinetic study of the dry reforming of propane over a $Ru/Al_2O_3$ catalyst. They observed zero-order rate dependence in propane and a fractional dependence in $CO_2$ and concluded that $CO_2$ is involved in the rate-determining step of the reaction.

In the work reported here, a 1.9 wt% Ni/Mg(Al)O, hydrotalcite-derived catalyst is studied for the dry reforming of propane at 600 °C. A primary target is to elucidate the role of the metal and of the support in the reaction cycle and to obtain key information on what makes these materials superior to conventional reforming catalysts. A TAP-II reactor system is used for isotopic labelling studies, and an ordinary fixed-bed reactor system is used for activity and stability measurements. Characterisation of the catalyst is carried out by magnetic measurements, in situ diffuse reflectance infrared Fourier transform spectroscopy (DRIFTS), and transmission electron microscopy (TEM) measurements.

## 2. Experimental

### 2.1. Catalyst preparation and general characterisation

The Ni/Mg(Al)O catalyst was prepared first by synthesis of the corresponding hydrotalcite-like material with nominal composition $Mg_{5.88}Ni_{0.12}Al_2(OH)_{16}CO_3 \cdot nH_2O$ and $(Mg + Ni)/Al = 3$ by coprecipitation at constant pH ($11.5 \pm 0.1$) and temperature ($40 \pm 2$ °C) in a specially designed apparatus. During synthesis the two reactant solutions, A [0.05 mole $CO_3^{2-}$/0.75 mole $OH^-$ with $K^+$; ≈ 750–800 ml] and B [0.25 mole cations ($Mg^{2+} + Ni^{2+} + Al^{3+}$) with $NO_3^-$; 250 ml], and the product solution (initially containing 500 ml distilled water) were kept at constant temperature in a water bath. The pH was controlled through a feedback loop with the use of a pH meter (Mettler Toledo 2220 with electrode Mettler Toledo INPRO 4500 Pt1000), which activated or stopped the pump (Watson/Marlow 101U/R) for the source solution A. Source solution B was added at a constant rate to the product solution via a second pump. The mixing of reactant solutions to yield the product solution was completed within approximately 150 min, followed by a stirring period of 60 min. The product obtained was washed and dried overnight at 90 °C. Phase purity of the obtained hydrotalcite-like phase was confirmed by means of powder X-ray diffraction (XRD). It is anticipated that the coprecipitation process at constant pH ensures a homogeneous distribution of nickel in the hydrotalcite-like material. The hydrotalcite-like material was converted into the catalyst by calcining and reducing it in one step by fluidising in 10% $H_2$ in $N_2$ for 14 h at 650 °C before cooling to ambient temperature under the same atmosphere. The reduced metal was then passivated for 1 h by passing 2% $O_2$ in $N_2$ over the material. Since the metal loading of the material is low, only a very small temperature increase was noticed during passivation. The passivated catalyst shows powder XRD reflections corresponding to a defect mixed cubic Mg(Al)O oxide (see Fig. 1A). In addition, a left-hand shoulder (indicated by an arrow) is observed for the reflection indexed as 111 ($d \approx 2.43$) for MgO, which does not belong to the mixed cubic Mg(Al)O structure. Rebours et al. [6] attribute the additional reflection to the presence of cations on tetrahedral sites in the cubic Mg(Al)O structure or in a defect spinel-like structure.

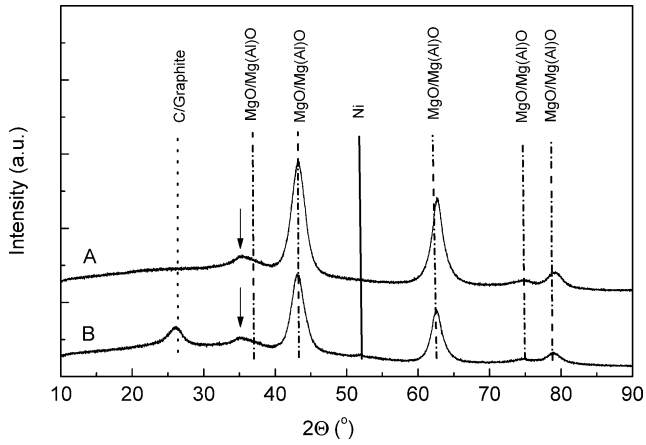


Fig. 1. Powder X-ray diffractograms of the 1.9 wt% Ni/Mg(Al)O catalyst before (A) and after catalytic testing (B) for 34 days at 600 °C. The composition of the feed in volume % is $C_3H_8$:$CO_2$:$H_2$:$N_2$ = 10:30:10:50.

The chemical composition with respect to Mg, Al, and Ni of the catalyst was determined by means of ICP–AES to be $(Mg + Ni)/Al = 3.2$. The metal loading of Ni/Mg(Al)O was determined to be 1.9 wt%. The BET surface area of the calcined material kept under inert conditions was 259 $m^2/g$.

### 2.2. Magnetic measurements

Magnetic measurements were performed at ambient temperature by the Weiss extraction method [7] in an electromagnet that supplied a field up to 21 kOe. Information on the degree of Ni reduction and on the mean surface diameter of the Ni metal particles ($D$) can be extracted from the magnetisation isotherm [8]. The degree of Ni reduction is calculated from the saturation magnetisation ($M_s$). For ferromagnetic materials, a residual magnetic moment remains at zero field after being exposed to a magnetic field. However, when the particle diameter goes below a certain size ($D_c$) the ferromagnetic particles become superparamagnetic [8]. The absence of remanent magnetisation ($M_r$) indicates superparamagnetic behaviour [8]. Under such conditions the mean sizes of large ($D_1$) and small ($D_2$) Ni particles can be calculated according to the Langevin equation [8]. The accuracy of the method is assumed to be within ±20% [7]. The mean surface diameter is calculated by $D = (D_1 + D_2)/2$. It is empirically determined that $D_c$ for Ni is 15 nm and that the ratio $2M_r/M_s$ gives the fraction of particles with a size

larger than the critical diameter in the applied magnetic setup (at IRC).

The average metal particle size found from magnetic measurements may be used to calculate the available metal surface area of a Ni catalyst. Since NiO and Ni–C are not ferromagnetic and therefore not detectable by this method, it was decided to study the fresh catalyst under a reducing atmosphere to determine the initial Ni surface area of the Ni/Mg(Al)O catalyst.

The passivated Ni/Mg(Al)O sample (190 mg) was loaded in a specially designed fixed-bed reactor used as sample holder in the electromagnet. The catalyst was heated in this reactor in an external furnace in a flow of 20% $H_2$ in $N_2$ from ambient temperature to 600 °C at a heating rate of 10 °C/min and a total flow rate of 70 Nml/min. When it reached 600 °C the reactor was rapidly taken out of the furnace and cooled to room temperature before it was loaded into the electromagnet for magnetisation measurements. Thereafter the reactor was put back into the furnace (at 600 °C) and heated for another hour before the next measurement was carried out (after cooling). A total of four magnetisation isotherm curves were collected after the catalyst had been exposed to 20% $H_2$ in $N_2$ at 600 °C for 0, 1, 2, and 3.5 h. Each measurement took approximately 1 h, including cooling the reactor to room temperature and heating it back to 600 °C after collection of the magnetisation isotherm curve.

### 2.3. Fixed-bed reactor testing

Activity and stability tests of the catalyst were performed in quartz tubular fixed bed reactors (i.d. 10 or 6 mm). The test temperature was measured with a thermocouple placed axially in the reactor inside a quartz thermocouple well (o.d. 3 mm). The reactor effluent was analysed by on-line gas chromatographic (GC) analysis (Agilent micro-GC equipped with three columns). The catalyst was tested with the use of either 1050 mg of catalyst (grain size 0.2–0.5 mm), with a total gas flow rate of 55 Nml/min and a feed gas with the composition (in vol%) $C_3H_8$:$CO_2$:$N_2$ = 20:60:20 (test I), or 450 mg of catalyst (grain size 0.2–0.5 mm), with a total gas flow rate of 100 Nml/min and a feed gas with the composition (in vol%) $C_3H_8$:$CO_2$:$H_2$:$N_2$ = 10:30:10:50 (test II). In both cases, the passivated catalyst was loaded into the reactor and heated to 600 °C under flowing $N_2$ and then exposed directly to the feed gases when it reached 600 °C. Test I was stopped after 27 h. Test II was stopped after 34 days. The XRD pattern of the catalyst tested for 34 days (test II) is shown in Fig. 1B, where the mixed Mg(Al)O phase can be identified together with carbon deposits and small amounts of reduced Ni. The Mg(Al)O carrier material, prepared and pretreated in the same manner as the catalyst, but without Ni, was tested for catalytic activity with the use of 450 mg of Mg(Al)O (grain size 0.2–0.5 mm), with a total gas flow rate of 100 Nml/min and a feed gas with the composition (in vol%) $CO_2$:$H_2$:$N_2$ = 30:10:60 or $C_3H_8$:$CO_2$:$H_2$:$N_2$ = 10:30:10:50. The activation energy of the Ni/Mg(Al)O catalyst for dry propane reforming was determined by temperature variation experiment in the temperature range 570–650 °C; all other test conditions were identical to those of test II.

### 2.4. Transmission electron microscopy measurements

TEM investigations were performed on a JEOL JEM 2010-FEG (EDX Link Isis). We prepared the sample by dispersing the catalyst ultrasonically in ethanol and depositing it on a holey carbon film supported on a copper grid. The Ni/Mg(Al)O sample was studied after passivation (see pretreatment description above) and after catalytic testing at 600 °C with a feed flow: $C_3H_8$:$CO_2$:$H_2$:$N_2$ = 10:30:10:50 (100 Nml/min) for 12 h.

### 2.5. In situ diffuse reflectance infrared Fourier transform spectroscopy

DRIFTS experiments were performed on a Nicolet IR 550 instrument equipped with an in situ DRIFTS cell from Spectratech. About 30 mg of catalyst with a grain size of 0.2–0.3 mm was used, and the experiments were carried out at 20 or 600 °C. Total flow rate was typically 50 Nml/min. All spectra were measured with a resolution of 4 $cm^{-1}$. Spectra of KBr under Ar at 20 °C or catalyst under Ar at 600 °C were used as a reference for background subtraction.

### 2.6. Temporary analysis of product experiments

Principles of the temporary analysis of product (TAP) experiments and their applications are described by Gleaves et al. [9]. Transient pulse experiments were carried out in a commercial TAP-2 reactor system (Mithra Technologies Inc.). The system is equipped with four high-speed pulse valves, a liquid trapped vacuum system, and a quadrupole mass spectrometer located directly underneath the microreactor (25.4 mm in length and 4.1 mm in diameter) exit. A heating element is wrapped around the microreactor, and a temperature controller reads the output of the thermocouple located in the catalyst bed. The reactor is typically loaded with 40 mg of 0.2–0.5-mm-size catalyst in the centre of the reactor between two layers of 0.2–0.3-mm-size quartz (210 mg). All experiments were started with an in situ $H_2$ reduction (10% $H_2$ in Ar, total flow rate 50 Nml/min, total pressure 1 atm) of the catalyst at 400 °C for 30 min. Then the system was evacuated and heated to 600 °C, at which point alternating pulse or multi-pulse experiments were carried out. The $^{12}C_3H_8$ + Ne pulse size was approximately 1 nmol ($6 \times 10^{14}$ molecules). During alternating pulse experiments, the size of the other pulse was adjusted so that the Ne amount was similar in the two pulses. This means that, for example, in alternating $^{12}C_3H_8$ + Ne (1:1)//$O_2$ + Ne (1:4) pulse experiments, the $^{12}C_3H_8$//$O_2$ ratio is 4:1.

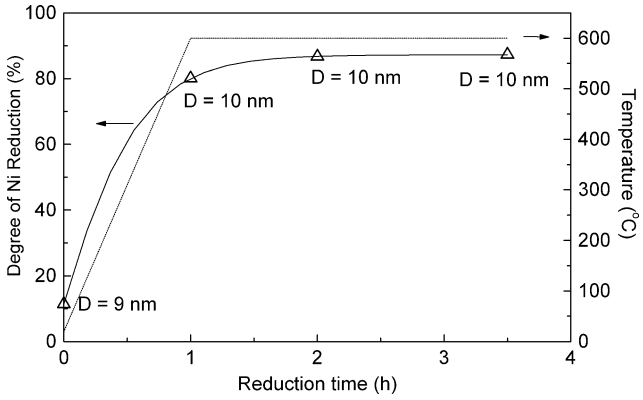


Fig. 2. Degree of Ni reduction and average nickel metal particle diameter ($D$) versus reduction time (20% $H_2$ in $N_2$) at 600 °C.

## 3. Results

### 3.1. Magnetic measurements

Fig. 2 shows the degree of Ni reduction versus reduction time (20% $H_2$ in $N_2$) for the catalyst. The passivated catalyst contains only ≈ 11% reduced Ni ($t = 0$; Fig. 2), with a calculated mean particle diameter ($D$) of $9 \pm 2$ nm. After heating to 600 °C (1 h reduction time; Fig. 2), the degree of reduction increases to ≈ 80% and $D$ increases to $10 \pm 2$ nm. After a 2-h reduction time (heat-up + isothermal conditions for 1 h), the degree of reduction was found to be 87%, and $D = 10 \pm 2$ nm. A further increase in reduction time (3.5 h in total) does not affect the degree of Ni reduction or the average particle diameter. The ratio $2M_r/M_s$ was calculated for all measurements, and less than 5% of the reduced nickel is found to be present as particles with a diameter larger than $D_c$ (15 nm). The stable fraction of nonferromagnetic nickel over the reduction experiment (about 13%) might be assigned to residual nickel ions in the solid solution phase MgNi(Al)O.

Based on the 1-h values (80% Ni reduction, $10 \pm 2$ nm average particle size), and assuming spherical particles, the Ni surface area of the catalyst was calculated to be 4 $m^2/g$, corresponding to $6 \times 10^{19}$ exposed Ni atoms per gram of catalyst.

### 3.2. Activity and stability tests

Results from two activity tests performed at 600 °C are shown in Figs. 3 A and 3B. Table 1 compares the experimental results with calculated equilibrium conversions and C selectivities under the applied conditions. Both experiments are performed far from equilibrium.

The first test (test I, Fig. 3A) was performed with a GHSV = 1560 $h^{-1}$ (based on total flow rate), leading to a high conversion for the title reaction:

$$C_3H_8 + 3CO_2 \rightarrow 6CO + 4H_2. \quad (1)$$

During the first hour on stream, the propane conversion surpasses the $CO_2$ conversion, and deactivation is observed.

Table 1
$C_3H_8$ and $CO_2$ conversion obtained at 600 °C under stabilised conditions and the corresponding conversion and carbon selectivity values calculated at thermodynamic equilibrium, accounting for carbon formation [10]. Thermodynamic data for graphitic C are used in the calculations

| | Feed conversion (%) | | C selectivity (%) |
|---|---|---|---|
| | $C_3H_8$ | $CO_2$ | |
| Test I—Gas composition (%): $C_3H_8$:$CO_2$:$N_2$ = 20:60:20 | | | |
| Experimental | 40 | 46 | |
| Thermodynamic equilibrium | 100 | 61 | 47 |
| Test II—Gas composition (%): $C_3H_8$:$CO_2$:$H_2$:$N_2$ = 10:30:10:50 | | | |
| Experimental | 10 | 30 | |
| Thermodynamic equilibrium | 100 | 57 | 45 |

The selectivity to methane and hydrogen decreases along with the propane conversion. The carbon balance of the experiment is 96% during the first GC analysis, increasing to $100 \pm 1$% after the fourth analysis (14 min on stream). This observation indicates initial deposition of carbon-containing products at the catalyst surface:

$$C_3H_8 \rightarrow C_xH_y + nH_2. \quad (2)$$

During the remaining 26-h test, the conversion and selectivity stabilise.

The $CO_2$ content of the reactor effluent is inversely related to the hydrogen content at any time in the experiment, and the $CO_2$ conversion is higher than the propane conversion after the first hour on stream. Together, these observations indicate that the reverse water gas shift reaction,

$$H_2 + CO_2 \leftrightarrow H_2O + CO \quad (3)$$

is rapidly equilibrating over the catalyst.

Another test performed with the same propane-to-carbon dioxide ratio, but with a much higher GHSV (not shown here), suffered from a rapid deactivation of the catalyst, leading to complete loss of activity after only 10 h on stream. The deactivation in this case is probably due to the oxidation of Ni particles by the feed, as indicated by a white catalyst colour after testing. We therefore performed a new stability test (test II), keeping the high GHSV (21200 $h^{-1}$, based on the total flow rate) but adding $H_2$ to the feed. The results of this test are shown in Fig. 3B. The stability test demonstrates that after a rapid and very limited deactivation (propane conversion decreases from 15 to 10% during the first hour on stream), the catalyst remains exceptionally stable under the applied test conditions, with even a slight increase in conversion over the whole test period of 34 days.

The carbon content of the catalyst, determined by combustion analysis after the long-term testing experiment (test II) in Fig. 3B, is 26 wt%. This carbon formation is confirmed by XRD analysis, showing a peak identified as carbon/graphite (Fig. 1B). Although the carbon content is significant, it corresponds to only 0.02% overall selectivity to carbon formation during the 34-day test (assuming a constant coking rate). This number is well below the predicted

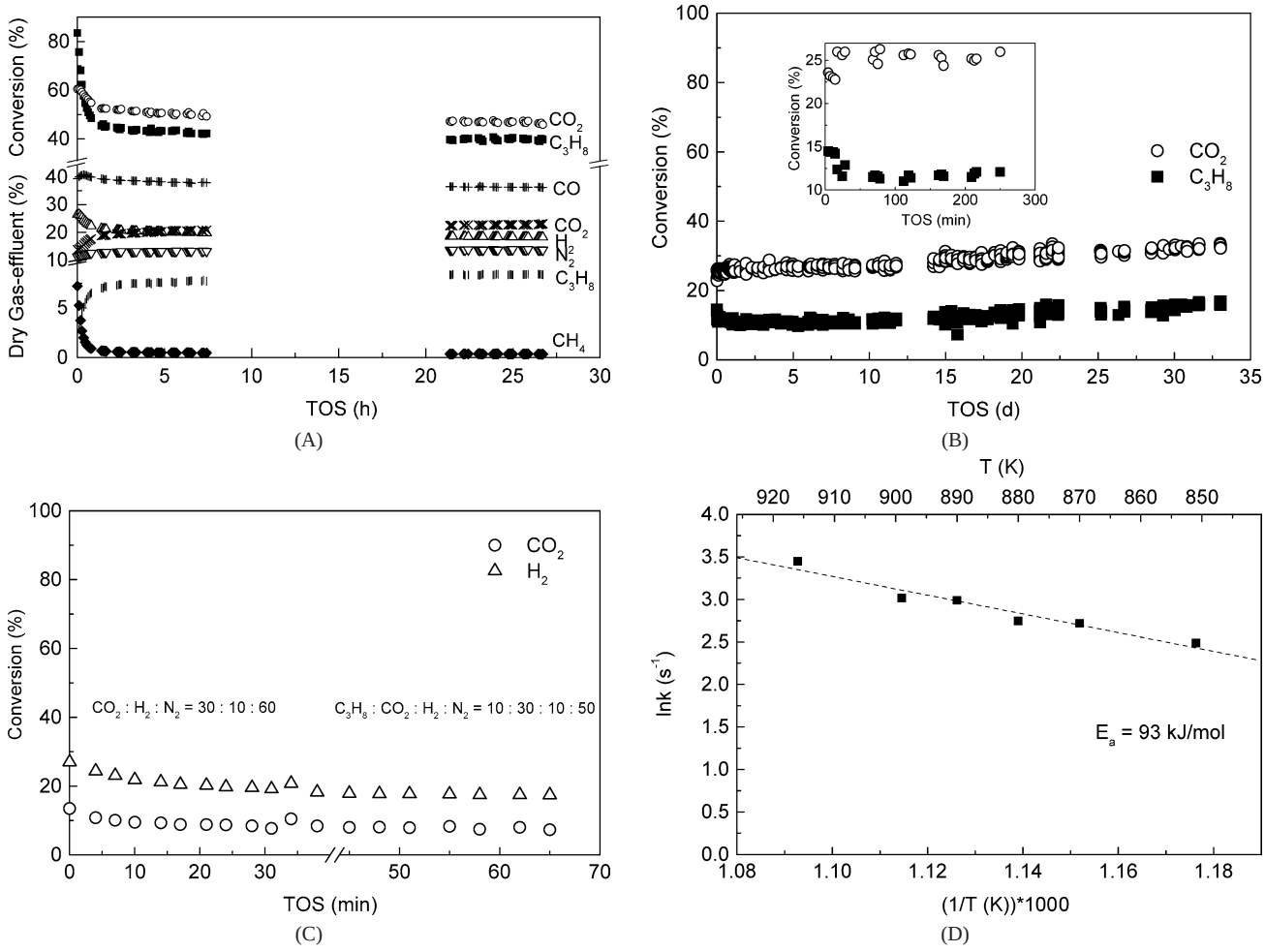


Fig. 3. (A) Activity test (test I) of 1.9 wt% Ni/Mg(Al)O under dry reforming conditions at 600 °C. The composition of the feed in vol. % is $C_3H_8$:$CO_2$:$N_2$ = 20:60:20. (B) Activity test (test II) of 1.9 wt% Ni/Mg(Al)O under dry reforming conditions at 600 °C. The composition of the feed in vol% is $C_3H_8$:$CO_2$:$H_2$:$N_2$ = 10:30:10:50. (C) Activity test of Mg(Al)O under RWGS and dry reforming conditions at 600 °C. The composition of the feed in vol% is $CO_2$:$H_2$:$N_2$ = 30:10:60 and $C_3H_8$:$CO_2$:$H_2$:$N_2$ = 10:30:10:50. (*D*) $\ln k$ versus $(1/T)$ plot for dry reforming of propane over the 1.9 wt% Ni/Mg(Al)O catalyst. The composition of the feed in vol% is $C_3H_8$:$CO_2$:$H_2$:$N_2$ = 10:30:10:50.

equilibrium [10] selectivity for graphitic carbon (Table 1) and indicates that the reaction kinetics at the Ni/Mg(Al)O catalyst is in favour of CO production.

Results from catalytic testing of the carrier material under reverse water gas shift (RWGS) or propane dry reforming conditions at 600 °C are shown in Fig. 3C. It can be observed that the carrier material is active for the RWGS reaction. The activity rapidly decreases with time on stream. It is worth noting that the reaction rate of the RWGS reaction is much slower on the carrier material than on the catalyst (Fig. 3A–3C). Addition of propane to the feed does not alter the CO production, but leads to negligible cracking of propane to methane and ethene (< 0.3% conversion). The empty reactor gives no conversion of $H_2$ or $CO_2$ under the same conditions.

The activation energy of the propane dry reforming reaction over the Ni/Mg(Al)O catalyst was determined to be 93 kJ/mol by a temperature variation experiment (Fig. 3D).

### 3.3. TEM

TEM images were collected for Ni/Mg(Al)O before and after catalytic testing under reforming conditions similar to those used in test II. The results are shown in Fig. 4. EDS analyses (spot size 25–50 nm) of the material showed a homogeneous average chemical composition (Mg/Al ≈ 3), indicating the absence of any phase segregation within the resolution of the measurements. For the passivated catalyst, the smaller particles (3 ± 2 nm) become visible in the thin areas of the sample (Fig. 4A) (depending on the contrast at imaging), whereas the larger ones (15 ± 5 nm) are observed in the thicker regions of the sample (Fig. 4B). The TEM images show a broad Ni particle size distribution before testing, ranging from approximately 1 nm to 20 nm, and indicate a random size distribution over the material. After catalytic testing (12 h), the sample is contaminated under the beam (becoming black because of positive ions trapped by the nonconducting sample), suggesting that it contains loosely bound hydrocarbons. There are still small particles on the

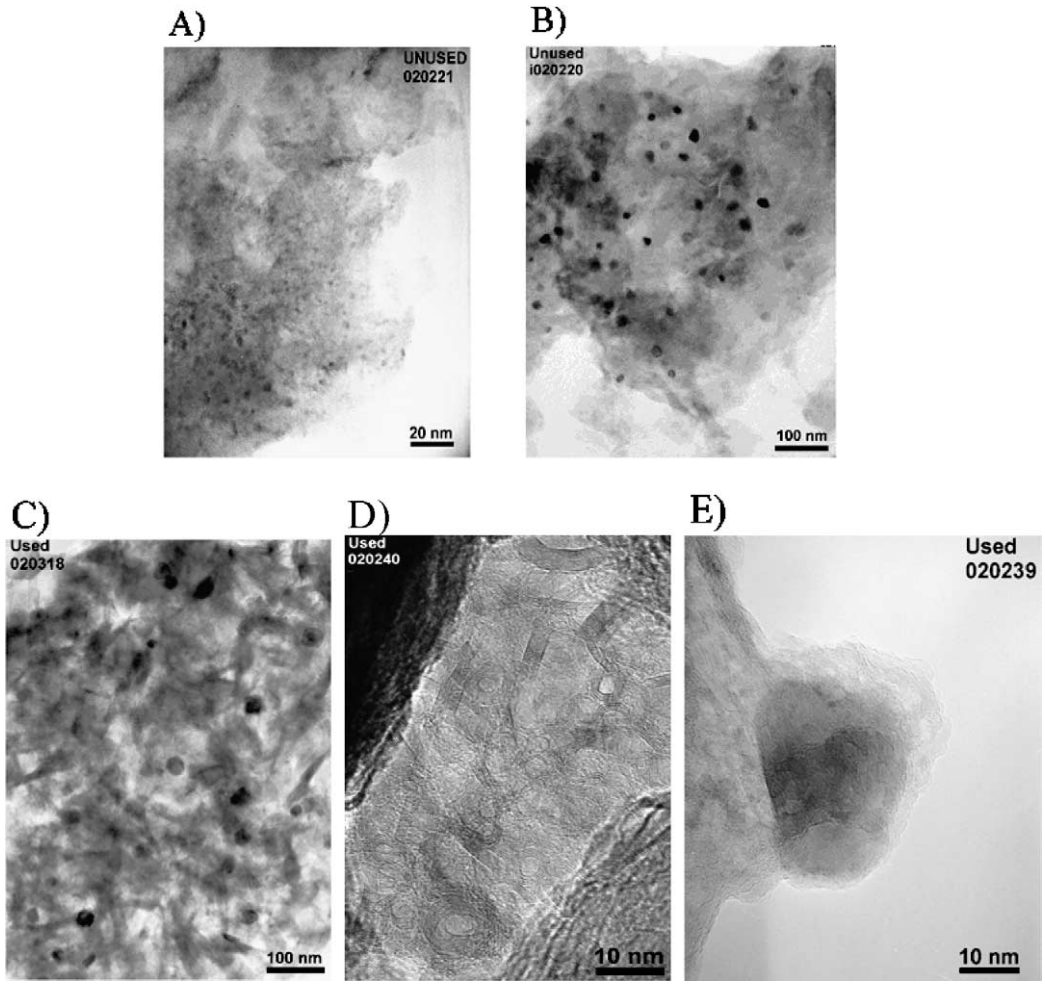


Fig. 4. TEM micrograph images of 1.9 wt% Ni/Mg(Al)O catalyst after passivation (A) and (B), after catalytic testing for 12 h under dry reforming conditions at 600 °C (C), carbon depositions in form of bi-dimensional and polymorphous carbon veils (D), and Ni-crystals mould into the basic mixed oxide support (E).

sample, but they could not be investigated because the signal was too noisy. The average diameter of the observed larger particles is $> 25$ nm (see Fig. 4C). For the tested catalyst, carbon deposits are observed in the form of bidimensional and polymorphous carbon veils that are formed along the surface, as revealed in Fig. 4D. The carbon deposits can also be seen as darker regions on the support (Fig. 4C). No hollow carbon filaments were observed by TEM analysis of the tested catalyst.

(Partial) coating of the nickel phase by the basic Mg(Al)O support is observed for some metal particles on the tested catalyst (Fig. 4E). The chemical composition of the coating was confirmed by EDS analysis. Migration of a Mg(Al)O carrier material onto metal particles has previously been reported for a Pd/Mg(Al)O catalyst [11].

### 3.4. *In situ DRIFTS*

Fig. 5 displays the DRIFT spectra of the passivated catalyst at ambient temperature under flowing Ar (spectrum A) and after heating to 600 °C under Ar (spectrum B) in the region between 4000 and 650 $cm^{-1}$. A selected part of spectra A and B is shown in the inset. The inset also shows a selected part of the DRIFT spectra of the catalyst after cooling to ambient temperature under flowing Ar after the heat treatment (spectrum C) and of the catalyst at 600 °C under 15% $CO_2$ in Ar + He (spectrum D). For all spectra but D, KBr spectra under flowing Ar at the respective temperatures are used for background. Details concerning spectrum D are discussed later in the text.

The passivated catalyst (spectrum A) shows broad bands/groups of bands in three frequency regions, $\approx$ 3700–2500 $cm^{-1}$ (region 1), $\approx$ 1800–1200 $cm^{-1}$ (region 2), and below 1200 $cm^{-1}$ (region 3). The most dominant bands in region 3 are related to lattice vibrations of the mixed oxide and will not be discussed further here. Spectrum A exhibits many similarities with FT-IR spectra published for the corresponding hydrotalcite-like phase [12,13]. As for the corresponding (Mg–Al)-hydrotalcite, frequencies in region 1 are assigned to hydroxyl stretching bands. Bands in region 2 are due to interlayer/physically adsorbed water, which gives rise to the band at $\approx$ 1650 $cm^{-1}$ [12,13]. The shoulder at 1750 $cm^{-1}$ may be assigned to adsorbed water, most likely in tight interaction with interlayer/adsorbed $CO_3^{2-}$

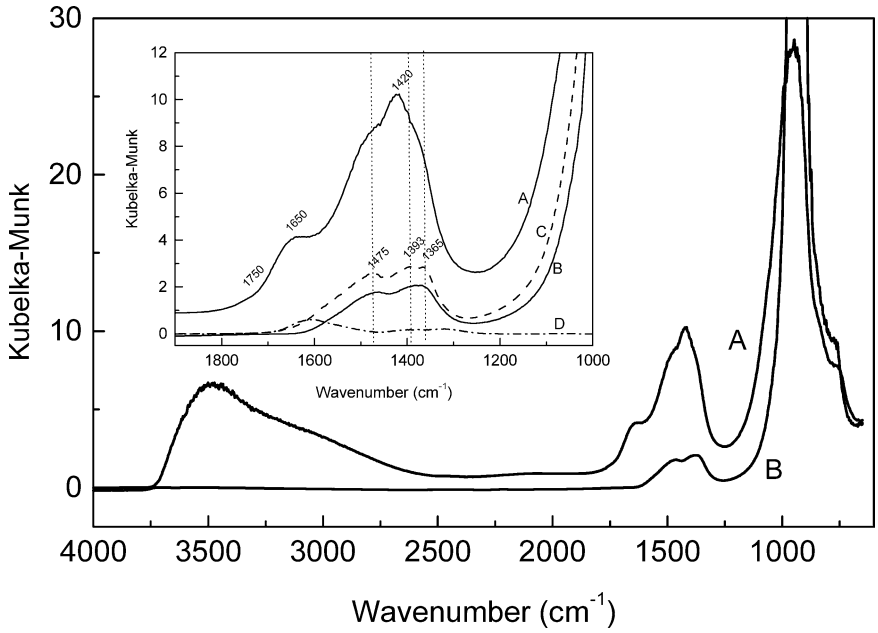


Fig. 5. DRIFT spectra of passivated 1.9 wt% Ni/Mg(Al)O at room-temperature (A) and heated to 600 °C under an Ar-flow (B). Inserted are details of selected parts of spectra (A) and (B) together with spectra collected for the catalyst cooled to room-temperature after heat-treatment to 600 °C under an Ar-flow (C) and under 15% $CO_2$ in Ar + He at 600 °C (D). For all spectra but (D), KBr under flowing Ar is used for background. For spectrum D the catalyst at 600 °C under Ar is used for background.

and hydroxyl groups on the brucite-like layers [13]. A multiple band is observed with a maximum at ≈ 1420 $cm^{-1}$. As the catalyst is heated under flowing Ar to 600 °C (spectrum B), bands in the hydroxyl stretching region are strongly decreased, and bands of interlayer/adsorbed water vanish as expected. Another strong change in the spectrum is observed in the 1800–1200 $cm^{-1}$ range with the disappearance of the band at 1420 $cm^{-1}$, and new bands appear at 1475, 1393, and 1365 $cm^{-1}$ (spectrum B), which are still more resolved after the catalyst is cooled to room temperature (spectrum C). It should be noted that the band at 1475 $cm^{-1}$ has a left-hand shoulder. Following the Herzberg notation [14], all of these bands are assigned to $\nu_3$ vibrations (asymmetric stretch) of different carbonate configurations. More details with respect to the carbonate bands are given below. In short, it may be concluded that the passivated catalyst (spectrum A) has partly recovered (memory effect) by adsorbing water and carbon dioxide during storage at ambient conditions. Even after heat treatment at 600 °C for 1 h in the DRIFTS cell (spectra B and C), some carbonate residues are present. The situation shown in spectra B and C should be considered to be the state of the surface prior to catalytic testing.

Figs. 6 and 7 display the DRIFT spectra of the catalyst under reforming conditions (10% $C_3H_8$ and 30% $CO_2$ in Ar + He) for 3 h and under 15% $CO_2$ in Ar + He at 600 °C in the frequency region between 4000 and 1000 $cm^{-1}$. Reference/background spectra are taken after the catalyst is heated to 600 °C under flowing Ar for 1 h. Details of the spectra are shown in the insets.

(i) Under reforming conditions, C–H bands related to gaseous propane and possibly to reforming intermediate (ethane, ethene, propene) or final (methane) products are observed at ca. 2950 ± 100 $cm^{-1}$ (Fig. 6, inset I). From the similarity observed between the pure gas-phase spectrum and this spectrum recorded under reforming conditions, it can be deduced that the possible accumulation of reaction intermediates (e.g., $C_xH_y$ adspecies) on the reacting catalyst is small on the time scale studied here (3 h). A weak doublet characteristic of gaseous CO [15], synthesised under reforming conditions, is observed at 2174 and 2111 $cm^{-1}$ (Fig. 6).

(ii) In Fig. 6 (inset II) and Fig. 7 (inset I) a multiple band with at least six maxima is observed in the frequency region ≈ 2360–2300 $cm^{-1}$. Two main bands of this ensemble may be assigned to the doublet of gaseous carbon dioxide, most likely the bands at 2358 and 2343 or 2332 $cm^{-1}$, which is close to what is normally reported in the literature (e.g., [15]). The other bands are also assigned to gaseous $CO_2$, since we observe the same splitting when passing gaseous $CO_2$ diluted in Ar over KBr at 400 °C in the DRIFTS cell. In both spectra shown in Figs. 6 and 7 (inset II), four very weak but sharp bands are observed in the frequency region ≈ 3740–3590 $cm^{-1}$. According to Ref. [16], gaseous carbon dioxide combination bands appear in the frequency regions 3734–3682 and 3640–3579 $cm^{-1}$. In a separate experiment (IR gas cell), we determined the combination bands for $CO_2$ to be at 3728, 3705, 3627, and 3601 $cm^{-1}$, which corresponds with what was observed in the DRIFT cell for the catalyst under inves-

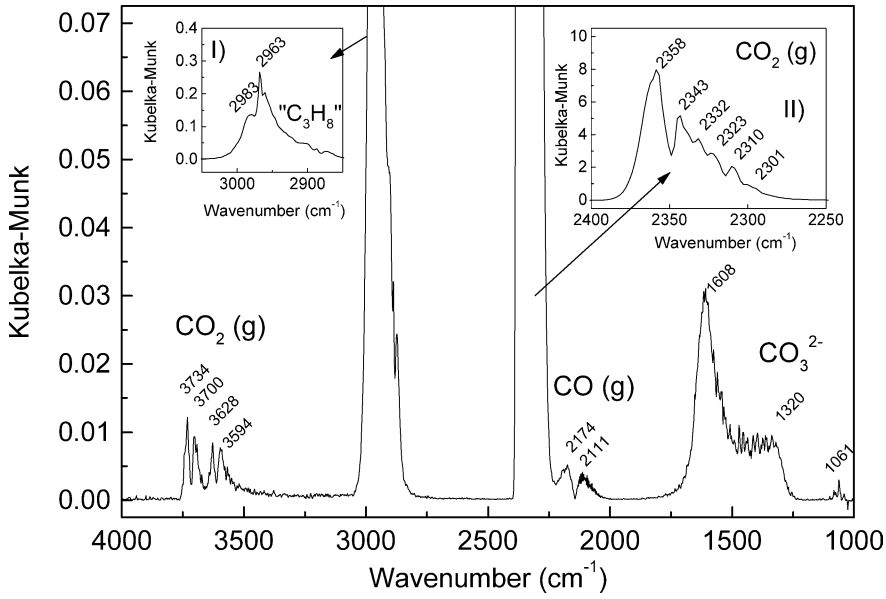


Fig. 6. DRIFT spectra of 1.9 wt% Ni/Mg(Al)O under dry reforming conditions at 600 °C. The catalyst at 600 °C under Ar is used for background.

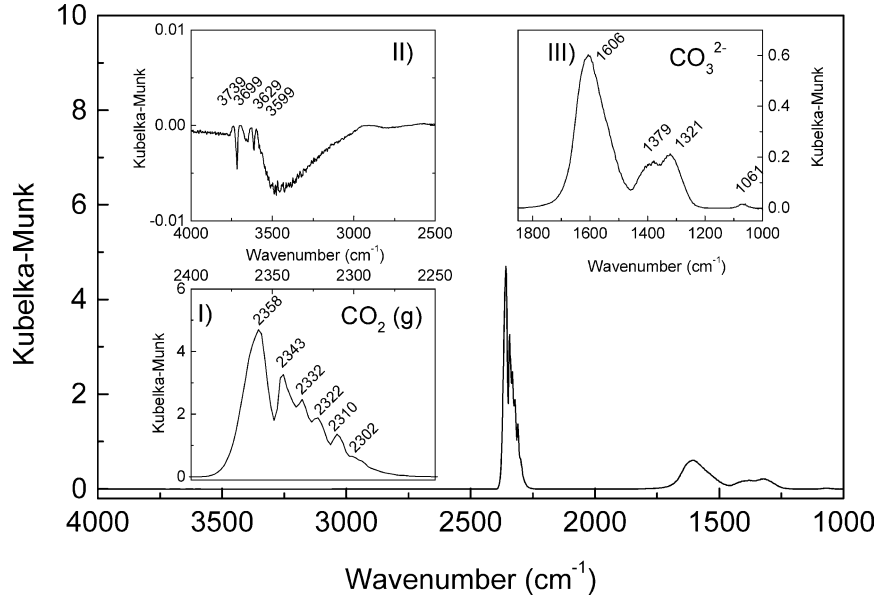


Fig. 7. DRIFT spectra of 1.9 wt% Ni/Mg(Al)O under 15% $CO_2$ in Ar + He at 600 °C. The catalyst at 600 °C under Ar + He is used for background.

tigation. In addition, a negative Kubelka–Munk (KM) signal is developing on the baseline of the spectra collected under 15% $CO_2$ in Ar + He (Fig. 7, inset II), indicating that hydroxyl species present in the background spectrum have disappeared under the reacting gas mixture.

(iii) For the catalyst working under 15% $CO_2$ in Ar + He at 600 °C, bands are observed at 1606 + right-hand shoulder, 1379, 1321, and 1061 $cm^{-1}$ (Fig. 7, inset III). Similar bands, with lower intensity and with more noise, are also observed in the spectra collected under reforming conditions (Fig. 6). All of these bands originate from carbonate formation on the defect mixed oxide. The $\nu_1$ vibration observed at 1061 $cm^{-1}$ also agrees with values in the literature [12,13]. The activation of the $\nu_1$ vibration requires that the carbonate ion not possess full symmetry. For that reason a splitting of the $\nu_3$ vibration should be expected. The quadruplet composed of a band at 1606 and its right-hand shoulder and the bands at 1379 and 1321 $cm^{-1}$ are interpreted to be due to $\nu_3$ vibrations of different carbonate ion configurations. According to Kloprogge et al. [12], only a $\nu_3$ doublet at 1401 and 1365 $cm^{-1}$ is observed for the corresponding (Mg–Al)-hydrotalcite. In the present work we observe differences in both frequencies and intensities (Figs. 5–7) of the carbonate group $\nu_3$ vibrations

due to the interaction of the carbonate ions with the mixed oxide. Carbonate groups can be located on regular interlayer sites, as in the hydrotalcite-derived catalyst (memory effect), or they can be located on less regular sites (adsorbed) with a less symmetric electrostatic interaction and giving rise to band splitting. In short, it can be concluded from the presented DRIFT spectra that carbonate groups are the major carbon-containing adsorbed species accumulating on the working catalyst under $CO_2$ in Ar + He or under reforming conditions ($CO_2$ and $C_3H_8$ in inert atmosphere for 3 h) at 600 °C. These carbonate groups are most likely located on different sites at the defect mixed Mg(Al)O structure, giving rise to multiple bands. The other carbon-containing adspecies necessarily involved in the catalytic process are not stable and/or abundant enough to be detected by IR spectroscopy.

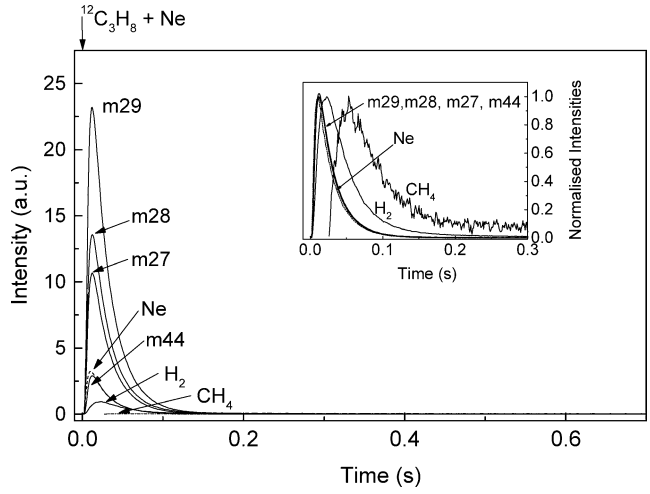


Fig. 8. Multiple pulse experiment, $^{12}C_3H_8$ + Ne (1:1) over 1.9 wt% Ni/Mg(Al)O (40 mg) at 600 °C.

### 3.5. TAP studies

TAP studies were performed with 40 mg of catalyst. Based on magnetic measurements of the fresh catalyst, this amount corresponds to $2 \times 10^{18}$ exposed Ni atoms. Based on the BET surface area of the material, the amount of exposed MgO entities is approximately $10^{20}$.

#### 3.5.1. $^{12}C_3H_8$ + He (1:1)

Results from experiments consisting of a series of pulses of $^{12}C_3H_8$ + Ne are shown in Fig. 8. The propane conversion is less than 10%. Normalised peaks (inset in Fig. 8) corresponding to masses 29, 28, and 27 all have the same shape as mass 44 (unique for propane in this case). Masses 29, 28, and 27 are all fragments of propane, but in addition they are characteristic peaks for propene, ethane, and ethene. The pulse shapes indicate that there is no desorption of $C_2$ and $C_3$ products from the active surface under TAP conditions. In addition, a delay in masses 16 and 2 compared with mass 44 (and 27, 28, and 29) is observed. Mass 16 is characteristic for methane, whereas mass 2 is characteristic for hydrogen (masses 2 and 16 are minor masses for propane, and a correction for the contribution of propane is applied). The normalised response of methane (peak maximum at 0.06 s) is delayed compared with hydrogen (peak maximum at 0.02 s). Tailing of $H_2$ is observed. Hydrogen production may take place directly in the gas phase or via surface intermediates. The delay in the $H_2$ peak compared with the propane peak means that at least some of the hydrogen is adsorbed to the surface, either as Ni–H species or as Ni–$C_xH_y$ species. The delay of methane compared with $H_2$ indicates it is formed from Ni–H species and/or that Ni–C species must be dispersed on the surface before methane can be formed. The absence of any delay in masses representing $C_2$ and $C_3$ products indicates that possible intermediate $C_2$ and $C_3$ alkanes/alkenes either are not formed or eventually dissociate further into $C_1$ species on the Ni surface. This observation is in agreement with data obtained under steady-state conditions already described (Fig. 3A and 3B) and differs from the observations reported by Solymosi et al. [4] for propane dissociation over a $Rh/Al_2O_3$ catalyst at 550–650 °C. In the case of $Rh/Al_2O_3$, propene was the major product, followed by ethene and methane.

#### 3.5.2. $^{12}C_3H_8$ + Ne (1:1)//$O_2$ + Ne (1:4)

Results from alternating $^{12}C_3H_8$ + Ne//$O_2$ + Ne pulse experiments are shown in Fig. 9. The propane conversion is approximately 50%. The oxygen conversion is complete. Product formation takes place on the propane pulse. Only CO and $H_2$ production is observed, and no formation of $CO_2$ was detected during the experiment. The hydrogen peak has its maximum at 0.02 s, which is similar to what is observed when only propane is pulsed (Fig. 8). Some tailing is observed for the $H_2$ peak. The CO peak is delayed compared with the $H_2$ peak, with a maximum at 0.03 s. It is interesting to note that the $H_2$ production in this experiment is about the same as in the "propane only" experiment already mentioned, in spite of the much higher propane conversion observed in the $^{12}C_3H_8$//$O_2$ case. This result could only be explained by water formation during the $^{12}C_3H_8$//$O_2$ experiment. The oxygen content in the feed pulses ($^{12}C_3H_8$:$O_2$ = 4:1) is only enough to oxidise 25% of the hydrogen in the Ni–$C_xH_y$ species to water. This result does imply that carbon residues are formed on the catalyst during the experiment. The number of molecules in each pulse ($\sim 10^{15}$ molecules) is so small compared with the exposed Ni surface ($\sim 10^{18}$ atoms) that the catalyst can be envisaged to be unchanged during the pulse series, even if all carbon was deposited. Still, it is interesting to note that the CO formation rate is unchanged during and after the $O_2$ pulse, whereas it increases steeply during/after the subsequent propane pulse.

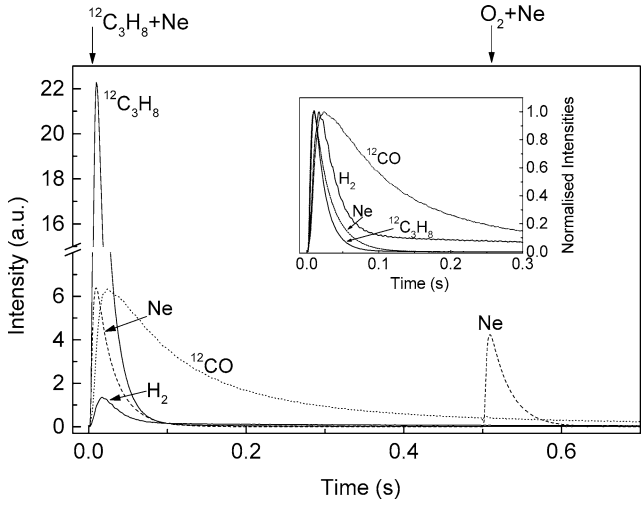


Fig. 9. Double pulse experiment, $^{12}C_3H_8 + Ne$ (1:1) followed by $O_2 + Ne$ (1:4) over 1.9 wt% Ni/Mg(Al)O (40 mg) at 600 °C.

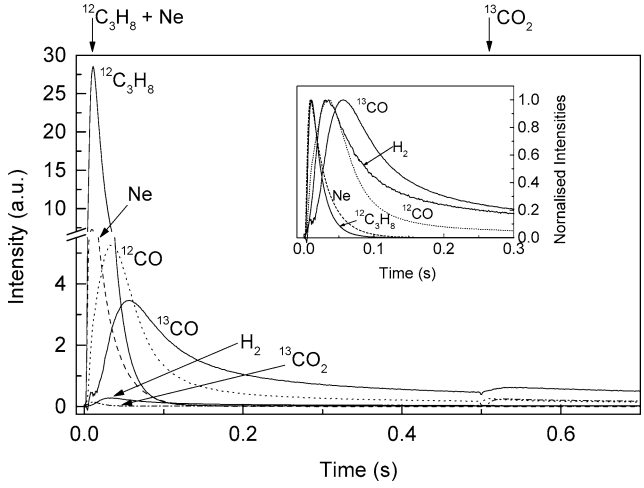


Fig. 10. Double pulse experiment, $^{12}C_3H_8 + Ne$ (1:1) followed by $^{13}CO_2$ over 1.9 wt% Ni/Mg(Al)O (40 mg) at 600 °C.

### 3.5.3. $^{12}C_3H_8 + Ne$ (1:1)//$^{13}CO_2$

Results from alternating $^{12}C_3H_8 + Ne//^{13}CO_2$ pulse experiments are shown in Fig. 10. The $^{12}C_3H_8$:$^{13}CO_2$ ratio in the pulses is approximately 3. The propane conversion is approximately 50%. The $CO_2$ conversion is > 99%. The $H_2$ production is even lower than in the $^{12}C_3H_8//O_2$ experiment above, implying significant water formation also in this case.

The major part of CO formation takes place during and after the propane pulse. Furthermore, two CO peaks are observed: one corresponding to $^{12}CO$ originating from $^{12}C_3H_8$ and one corresponding to $^{13}CO$, originating from $^{13}CO_2$. Note that the $^{12}CO$ peak appears before the $^{13}CO$ peak, with peak maxima at 0.04 and 0.06 s, respectively. The tailing of the $^{12}CO$ peak is moderate and less pronounced than in the $^{12}C_3H_8//O_2$ experiment, whereas the $^{13}CO$ peak has long tailing. During the $^{13}CO_2$ pulse, only minor amounts of $^{13}CO_2$ are observed, indicating full sorption of $^{13}CO_2$. A slight increase in both the $^{13}CO$ signal and the residual $^{12}CO$ background is observed during the $^{13}CO_2$ pulse. Integration of the $^{12}CO$ and $^{13}CO$ signals during the time interval 0–0.5 s shows that their areas are similar in that time interval. However, the total area of the $^{13}CO$ peak (0–2 s) is close to 2 times the total $^{12}CO$ peak area. These numbers correspond to the following reaction stoichiometry:

$$2\,^{12}C_3H_8 + 6\,^{13}CO_2 \rightarrow {}^{12}C_3H_8 + 3\,^{12}CO + 6\,^{13}CO + 3H_2O + H_2. \quad (4)$$

## 4. Discussion

### 4.1. Catalyst activity and stability under steady-state conditions

The initial turnover frequency (TOF) of the Ni/Mg(Al)O catalyst for propane dry reforming at 600 °C was calculated from the results shown in Fig. 3B, with the use of the initial Ni surface area calculated from magnetic measurements (4 $m^2/g$). The resulting TOF value was 0.22 molecules/(site s). This value is lower than reported in the literature for methane dry reforming over similar catalysts; Rostrup-Nielsen and Bak Hansen [17] reported a TOF value of 1.9 molecules/(site s) and 2.7 molecules/(site s), for Ni supported on MgO and $MgAl_2O_4$, respectively, at 550 °C. Using the activation energy determined for our reaction-catalyst system (93 kJ/mol), we calculated the TOF of our catalyst for propane dry reforming to be 0.1 molecules/(site s) at 550 °C. This value is less than 5% of the TOF values reported by Rostrup-Nielsen and Bak-Hansen for methane dry reforming [17]. The propane dry reforming data obtained under TAP conditions (Fig. 10) show that the intrinsic reaction rate is higher than observed under steady-state conditions. During alternating pulse experiments, the CO peak maximum is observed 0.03 s after the propane pulse, and the calculated residence time at 600 °C is $\tau = (1/\mathrm{TOF}) = 4.5$ s under steady-state conditions. Together, these data indicate that the low TOF observed over our catalyst is most likely due to the inaccessibility of a large fraction of the Ni surface, either because it is partially decorated by the support (as observed by TEM, see Fig. 4E) or by carbon deposits (as indicated by the high carbon content of the used catalyst), or because the Ni surface is partially oxidised under reaction conditions. A more intrinsic explanation for a lower TOF for propane than for methane dry reforming is that propane activation may require larger ensembles of nickel atoms than methane, which may result in a lower sticking coefficient for propane dry reforming. Based on the results obtained in this study, none of these possibilities may be excluded.

Important processes that may cause catalyst deactivation are coke formation and metal particle sintering. Initial catalyst deactivation is observed during the first hour on stream for the catalyst under test conditions as described for tests I

and II. In the case of test I, a high propane conversion relative to the $CO_2$ conversion is observed together with a poor carbon mass balance during the first 14 min on stream. The close relationship between initial deactivation and poor C balance strongly suggests that coking plays an important part in the initial deactivation process. For test II, a higher $C_3H_8/CO_2$ conversion ratio is observed during the first hour on stream. Initial carbon deposit formation (12 h) was confirmed by TEM analysis (Fig. 4C and 4D). In addition, TEM reveals that Ni particle sintering takes place, at least on the larger Ni particles (going from $15 \pm 5$ nm to more than 25 nm; Fig. 4B and 4C). It is difficult to conclude whether coke formation or Ni particle sintering is the dominant reason for the initial catalyst deactivation, or if a combination of the two processes takes place under the applied test conditions (test II).

Another interesting observation is that the carbon content of the catalyst after 34 days of testing (test II) is 64 times the total Ni content of the catalyst, on a molar basis (26 wt%). This result, in combination with the observed stable activity of the catalyst after the first hour on stream and the absence of carbon whisker formation, may indicate that coke formation takes place on a limited number of Ni sites (most likely the large Ni particles, since small Ni particles ($< 2$ nm) have been reported to be inactive for coke formation during methane dry reforming [18]). The formed carbon film on the metal is spilled over to the support material, forming bidimensional and polymorphous carbon veils on the support during testing (Fig. 4C and 4D), maintaining a constant amount of active nickel sites.

The absence of carbon whiskers as revealed by TEM can also indicate that the Ni particles (essentially the small ones) are in intimate contact with the Mg(Al)O support. As a matter of fact, the generally agreed process for whisker formation involves diffusion of the deposited carbon on the active side of a particle through the Ni particle as Ni carbide and its extrusion at the other side, lifting the particle away from the support [19].

### *4.2. Propane dry reforming mechanism and role of carrier material in the catalytic cycle*

Since no detailed reaction mechanism for propane dry reforming has been published yet (most studies being devoted to methane dry reforming), we will start the discussion by giving an overview of methane dry reforming mechanisms proposed by other authors for similar systems. The interaction between the catalyst and $CO_2$, which has in all cases been studied by $^{12}CH_4//^{13}CO_2$ pulse experiments in the TAP reactor, will be the focal point of this overview.

The reaction mechanism over a $Ni/SiO_2$ catalyst is proposed to be [15]

$$CH_4 + Ni \leftrightarrow NiC + 2H_2, \quad (5)$$

$$CO_2 + Ni \leftrightarrow CO + NiO, \quad (6)$$

$$NiC + NiO \rightarrow CO + 2Ni. \quad (7)$$

Step (5) is considered to be fast, lumping several elementary steps, leading to accumulated carbon monomers. $CO_2$ dissociates on the metal surface into adsorbed oxygen and gaseous CO. In step (7) CO is formed from carbon and oxygen adspecies (from methane cracking and carbon dioxide dissociation). Step (7) is considered to be the rate-limiting step. The main observation leading to the proposal of step (6) is that $^{13}CO$ appeared before $^{12}CO$ in the $^{12}CH_4//^{13}CO_2$ pulse study, indicative of $^{13}CO_2$ splitting prior to $^{12}CO$ formation.

For a $Ru/SiO_2$ catalyst, a slightly different mechanism is proposed [20]:

$$CH_4 + Ru \leftrightarrow RuC + 2H_2, \quad (8)$$

$$CO_2 + RuC \leftrightarrow Ru + 2CO. \quad (9)$$

The methane activation step is identical to that observed for $Ni/SiO_2$, whereas $CO_2$ would interact directly with the metal carbide, without an intermediate partial oxidation of Ru, in step (9). The main observation leading to the proposal of step (9) is that $^{12}CO$ and $^{13}CO$ appeared simultaneously in the $^{12}CH_4//^{13}CO_2$ pulse study, indicative of simultaneous $^{13}CO_2$ splitting and $^{12}CO$ formation. Step (8) has been proposed to be the rate-limiting step [21].

For a $Ni/La_2O_3$ catalyst the following mechanistic route is proposed [22]:

$$CH_4 + Ni \leftrightarrow NiC + 2H_2, \quad (10)$$

$$La_2O_2CO_3 + Ni \rightarrow CO + NiO + La_2O_3, \quad (11)$$

$$CO_2 + La_2O_3 \rightarrow La_2O_2CO_3, \quad (12)$$

$$NiC + NiO \rightarrow 2Ni + CO. \quad (13)$$

Methane is activated on the metallic surface, whereas $CO_2$ interacts with $La_2O_3$ and forms $La_2O_2CO_3$, which subsequently oxidises Ni, leading to CO formation. Interaction between oxidised and carbided Ni then leads to formation of another CO, whereas the Ni particle is restored to its original state. In this case the CO precursor is stored as $La_2O_2CO_3$ outside the metal surface, and the Ni particles are decorated with layers of $La_2O_3/La_2O_2CO_3$. This mechanism is mainly based on the following observations. A DRIFTS study showed the presence of $La_2O_2CO_3$ on the catalyst surface during $CO_2$ reforming of methane. A SSITKA study, in which $^{12}CO_2$ is replaced by $^{13}CO_2$, strongly indicated that the $La_2O_2CO_3$ pool is participating in the reaction cycle. During a $^{12}CH_4//^{13}CO_2$ pulse experiment in the TAP reactor, the $^{12}CO$ production decreased during the $CH_4$ pulse, indicative of competitive adsorption at one common site. This last observation is crucial for the suggestion of step (11).

As will be seen from the following discussion, the Ni/Mg(Al)O catalyst used for dry reforming of propane in our study bears resemblances to all of the catalyst/reaction systems referred to above. However, it also shows important deviations from each of them. Below, each feature is presented and discussed:

1. $^{13}CO_2$ is completely adsorbed during the $^{13}CO_2$ pulse in the $^{12}C_3H_8//^{13}CO_2$ experiment and gives rise only to slow $^{13}CO$ formation. Such a feature has not been reported before (e.g., [15,20,22]).
   DRIFTS data reported above suggest that the Ni/Mg(Al)O catalyst acts as a $CO_2$ sorbent, forming carbonate species at basic sites. Several observations point to the support material as the adsorption site for $CO_2$, even under pulse experiments in the TAP reactor. First, the support surface of our catalyst is two orders of magnitude larger than the Ni surface. Second, the literature points to calcined hydrotalcite as a $CO_2$ sorbent under methane steam reforming conditions [23,24]. A $CO_2$ adsorption enthalpy of 140–150 kJ/mol on Mg(Al)O has been reported [25]. This value corresponds to a residence time of $10^{-4}$ s at 600 °C (assuming an adsorbate stretching frequency of $10^{13}$ $s^{-1}$ and not taking into account the entropy loss). From kinetic gas theory, the corresponding equilibrium $CO_2$ gas pressure is $10^{-9}$ atm, leading to a collision frequency with the solid surface of $10^{18}$ collisions/($m^2$ s) at 600 °C. These data indicate that the long residence times and slow decomposition rate observed for $CO_2$ on the Ni/Mg(Al)O catalyst may be due to a chromatographic effect, where $CO_2$ is constantly adsorbed and desorbed until it reaches a decomposition site.
   Few data have been published on the interaction between $CO_2$ and Ni metal. Galan et al. studied the interaction between Ni atoms and $CO_2$ at 10–106 K by UV and FTIR spectroscopy and density functional theory (DFT) calculations [26]. No Ni–$CO_2$ interaction could be observed when $CO_2$ was in the gas phase, even at this low temperature. When Ni and $CO_2$ were cocondensed, they were observed to display a weak Ni–$CO_2$ interaction. Already at 106 K, conversion of Ni–$CO_2$ to CO and NiO was observed, indicating a low activation energy for this reaction.
   Bligaard et al. recently published DFT calculations for $CO_2$ dissociative adsorption on a Ni(211) surface, reporting a slightly positive adsorption enthalpy of 16 kJ/mol [27]. This means that a driving force, such as a partial pressure ratio of $(P_{CO_2}/P_{CO}) > 9$, is needed to drive the reaction towards NiO. Such a driving force is easily achieved under TAP conditions, when $CO_2$ is pulsed over the catalyst in the absence of CO. If $CO_2$ were adsorbed on Ni, and not on the support, it would lead to CO formation mainly during the $CO_2$ pulse, as observed for the other supported metal systems referred to above [15,20,22]. Instead, the complete sorption of $CO_2$ observed during the $CO_2$ pulse over the Ni/Mg(Al)O catalyst, followed by slow CO release, strongly indicates that this is not the case. $CO_2$ is selectively adsorbed on the Mg(Al)O support:

$$CO_2 + O^{2-} = CO_3^{2-}. \quad (14)$$

2. Carbon species deposited on the catalyst during the propane pulse do not react during a subsequent oxygen pulse (Fig. 9).
   When $O_2$ disappears from the $O_2$ pulse without influencing the apparent product formation, we interpret this as formation of Ni–O species. Furthermore, when increased CO formation is observed during the subsequent propane pulse, this can be accounted for by reaction between propane and Ni–O. The hydrogen formation during the propane pulse is low and indicates water formation. Together, these results imply that after the $O_2$ pulse, Ni–O and Ni–C species are present on the catalyst, without giving rise to the expected CO formation.
3. Product formation is observed mainly during the propane pulse. This result is at variance with literature reports on methane dry reforming (see above), where CO formation takes place during the $CO_2$ pulse. A possible reason for this difference could be that in our case, propane is used as a reactant instead of methane. It is therefore likely that three Ni–C species are formed adjacent to each other, with a lower diffusivity/reactivity than single Ni–C species. Other speculative possibilities exist but will not be discussed because of lack of evidence.
   It is further interesting to observe that much higher propane conversion is observed in the presence of oxide species than in "propane only" experiments. This last observation is in line with literature reports [28] and indicates that propane reacts directly with oxide species to give CO and $H_2O$ (and $H_2$).
4. The oxygen pool in the $^{12}C_3H_8//O_2$ experiment reacts more rapidly than the oxygen pool in the $^{12}C_3H_8//^{13}CO_2$ experiment.
   This observation indicates that some of the oxygen pool in the $^{12}C_3H_8//^{13}CO_2$ experiment is present as carbonate species on the support, which continuously react to split off active oxygen species:

$$CO_3^{2-} \rightarrow CO + O^{2-} + O_{act}. \quad (15)$$

5. The initial slope of the $^{12}CO$ peak in the $^{12}C_3H_8//^{13}CO_2$ experiment is identical to the $^{12}CO$ peak in the $^{12}C_3H_8//O_2$ experiment.
   This observation indicates that the most rapid $^{12}CO$ formation in the $^{12}C_3H_8//^{13}CO_2$ experiment takes place by reaction between propane intermediates and Ni–O. A second implication of this result is that some $CO_3^{2-}$ has decomposed to Ni–O and CO prior to the propane pulse. This hypothesis is in agreement with the observation of an increase in the $^{13}CO$ production after the $^{13}CO_2$ pulse. Ni–O could be formed by direct interaction between $^{13}CO_3^{2-}$ (or its decomposition products) and Ni, or via the gas phase (the theoretical number of collisions between $^{13}CO_2$(g) and the catalyst surface under TAP conditions could indeed match the slow $^{13}CO$ evolution; see above).

6. $^{13}CO$ appears with a delay compared to $^{12}CO$ during the propane pulse in the $^{12}C_3H_8//^{13}CO_2$ experiment. Such a delay has not been reported before. This observation indicates that decomposition of carbonate is activated by the propane pulse. There are three possible explanations for this observation:
   (a) Easily accessible Ni sites are available for oxidation by $^{13}CO_3^{2-}$ after the initial $^{12}CO$ formation (with reduction of Ni–O). In this case, Ni oxidation by $^{13}CO_3^{2-}$ must take place by direct reaction at the rim of the Ni particles, since the rate of reaction between $CO_2$ in gas phase and the Ni surface will not be affected by the propane pulse ($\approx 10^{15}$ molecules compared with $\approx 10^{18}$ Ni atoms) (Eq. (15)). Subsequent reaction with hydrogen species (Eq. (16)) on the Ni surface would, together with Eq. (14), constitute the full RWGS cycle.

$$O_{act} + \text{“}H_2\text{”} \rightarrow H_2O. \quad (16)$$

   A direct oxidation of Ni to Ni–O species by $CO_3^{2-}$ at the rim, together with a low diffusivity of Ni–O, could also explain why oxidation of Ni (and release of $^{13}CO$) is slow in the absence of the propane pulse, but increases in rate when these Ni–O species are reduced.
   (b) An alternative reason for the propane-activated $^{13}CO$ formation may be that the surface of the Ni particles contains Ni–H species, which are able to react either with $CO_2$ in the gas phase or with carbonate at the rim of the Ni particle. Such a reaction would explain why $^{13}CO$ and $H_2$ are the main products at delays greater than 0.3 s in the $^{12}C_3H_8//^{13}CO_2$ pulse experiment.
   (c) A last possibility is that $H_2$ in the gas phase reacts with carbonate on the support. This is a possible reaction, as seen in Fig. 3C, but would be expected to have a low rate.

## 5. Conclusion

This study revealed that a nickel catalyst derived from hydrotalcite precursors exhibits an exceptional stability under propane dry reforming conditions, despite an important carbon formation. The absence of whisker formation, generally responsible for catalyst deactivation (due to particle fragmentation and encapsulation), is assumed to come from a strong metal–support interaction (including Ni particle partial decoration). The latter stabilises the nickel particles and favours oxidation of the Ni particles by the surrounding carbonates, which act as a permanent oxygen reservoir (under TAP conditions). Rapid CO (and water) formation is observed by interaction between propane and Ni–O species, and additional CO is formed by the following carbonate reduction.

## Acknowledgment

This study was supported by the Norwegian Research Council under the KOSK programme.

## References

[1] F. Cavani, F. Trifiro, A. Vaccari, Catal. Today 11 (2) (1991) 173.
[2] D. Tichit, B. Coq, Cattech 7 (6) (2003) 206.
[3] T. Shishido, M. Sukenobu, H. Morioka, R. Furukawa, H. Shirahase, K. Takehira, Catal. Lett. 73 (1) (2001) 21.
[4] F. Solymosi, P. Tolmacsov, K. Kedves, J. Catal. 216 (1–2) (2003) 377.
[5] D. Sutton, J.F. Moisan, J.R.H. Ross, Catal. Lett. (2001) 175.
[6] B. Rebours, J.B. d'Espinose de la Caillerie, O. Clause, J. Am. Chem. Soc. 116 (1994) 1707.
[7] P.W. Selwood, Chemisorption and Magnetization, Academic Press, New York, 1975.
[8] J.-A. Dalmon, in: B. Imelik, J.C. Védrine (Eds.), Catalyst Characterization, Physical Techniques for Solid Materials, Plenum Press, New York, 1994.
[9] J.T. Gleaves, G.S. Yablonskii, P. Phanawadee, Y. Schuurman, Appl. Catal. 160 (1997) 55.
[10] Thermodynamic calculations were performed using the Gibbs energy minimisation function of the “HCS Chemistry” software, available from http://www.outokumpu.com/hsc.
[11] M. Martinez-Ortiz, D. Tichit, P. Gonzalez, B. Coq, J. Molec. Catal. A: Chemical 201 (2003) 199.
[12] J.T. Kloprogge, R.L. Frost, J. Solid State Chem. 146 (1999) 506.
[13] J. Perez-Ramirez, G. Mul, J.A. Moulijn, Vib. Spectrosc. 27 (2001) 75.
[14] W.B. White, in: V.C. Farmer (Ed.), The Infrared Spectra of Minerals, Mineralogical Society, London, 1974.
[15] V.C.H. Kroll, H.M. Swaan, S. Lacombe, C. Mirodatos, J. Catal. 164 (1997) 387.
[16] International Union of Pure Applied Chemistry Commission on Molecular Structure and Spectroscopy, London Butterworths, 1961.
[17] J.R. Rostrup-Nielsen, J.-H. Bak Hansen, J. Catal. 144 (1993) 38.
[18] J.A. Lercher, J.H. Bitter, W. Hally, W. Niessen, K. Seshan, Stud. Surf. Sci. Catal. 101 (1996) 463.
[19] J.R. Rostrup-Nielsen, in: J.R. Anderson, M. Boudart (Eds.), Catalysis—Science and Technology, vol. 5, Springer-Verlag, Berlin, 1984.
[20] Y. Schuurman, V.C.H. Kroll, P. Ferreira-Aparicio, C. Mirodatos, Catal. Today 38 (1997) 129.
[21] M.F. Mark, W.F. Maier, J. Catal. 164 (1996) 122.
[22] Å Slagtern, Y. Schuurman, C. Leclercq, X. Verykios, C. Mirodatos, J. Catal. 172 (1997) 118.
[23] Y. Ding, E. Alpay, Chem. Eng. Sci. 55 (2000) 3461.
[24] Y. Ding, E. Alpay, Chem. Eng. Sci. 55 (2000) 3929.
[25] J. Shen, J.M. Kobe, Y. Chen, J.A. Dumesic, Langmuir 10 (1994) 3902.
[26] F. Galan, M. Fouassier, M. Tranquille, J. Mascetti, I. Pápai, J. Phys. Chem. A 101 (1997) 2626.
[27] T. Bligaard, J.K. Nørskov, S. Dahl, J. Matthiesen, C.H. Christensen, J. Sehested, J. Catal. 224 (2004) 206.
[28] O. Dewaele, G.F. Froment, J. Catal. 184 (1999) 499.